

# Accepted Manuscript

Structural-depth analysis of the Yola Arm of the Upper Benue Trough of Nigeria using high resolution aeromagnetic data

J.K. Ogunmola, E.A. Ayolabi, S.B. Olobaniyi



PII: S1464-343X(16)30302-8

DOI: [10.1016/j.jafrearsci.2016.09.008](https://doi.org/10.1016/j.jafrearsci.2016.09.008)

Reference: AES 2666

To appear in: *Journal of African Earth Sciences*

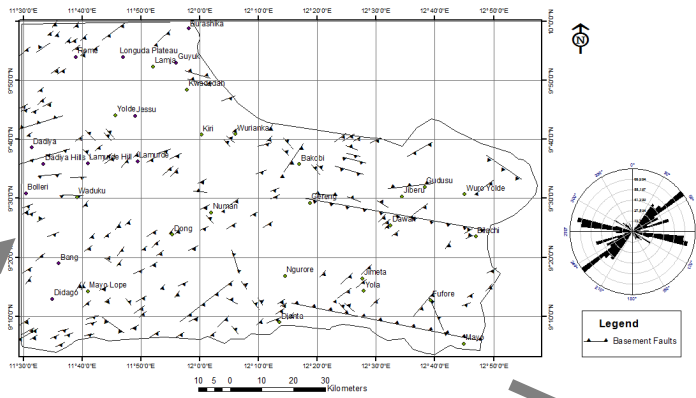
Received Date: 4 September 2015

Revised Date: 9 September 2016

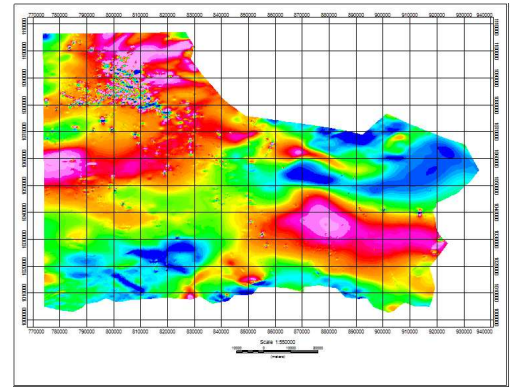
Accepted Date: 15 September 2016

Please cite this article as: Ogunmola, J.K., Ayolabi, E.A., Olobaniyi, S.B., Structural-depth analysis of the Yola Arm of the Upper Benue Trough of Nigeria using high resolution aeromagnetic data, *Journal of African Earth Sciences* (2016), doi: 10.1016/j.jafrearsci.2016.09.008.

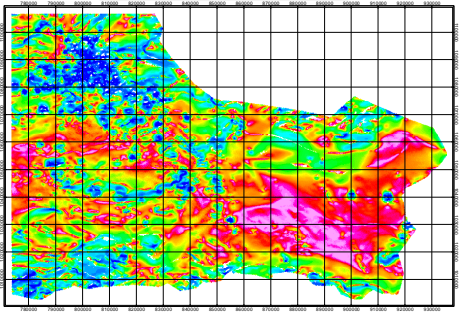
This is a PDF file of an unedited manuscript that has been accepted for publication. As a service to our customers we are providing this early version of the manuscript. The manuscript will undergo copyediting, typesetting, and review of the resulting proof before it is published in its final form. Please note that during the production process errors may be discovered which could affect the content, and all legal disclaimers that apply to the journal pertain.



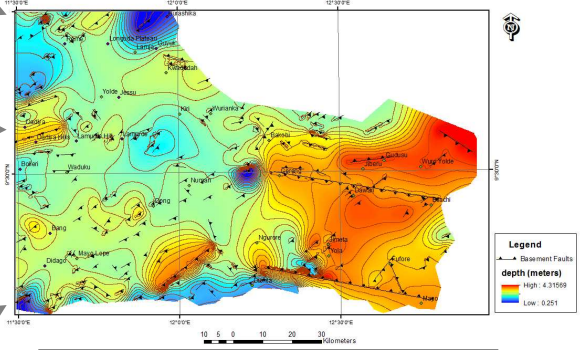
**BASEMENT FAULTS**



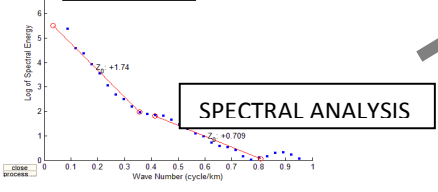
**GRID OF TOTAL MAGNETIC INTENSITY (TMI)**



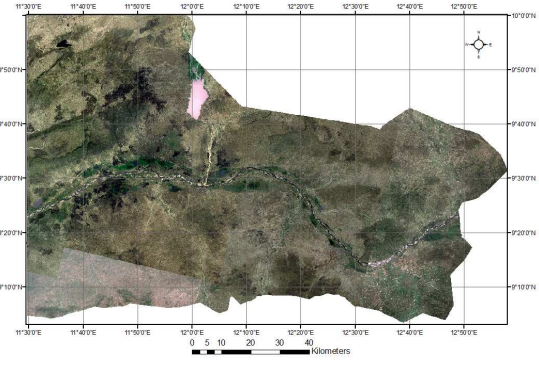
**SPI GRID**



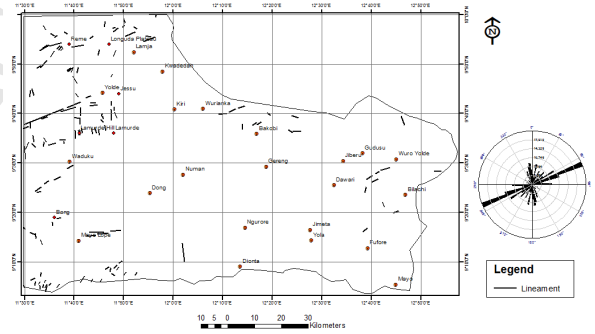
**DEPTH TO BASEMENT STRUCTURE MAP**



**SPECTRAL ANALYSIS**



**SPOT 5 IMAGE**



**LINEAMENTS FROM SPOT 5**

1     **Structural-Depth Analysis of the Yola Arm of the Upper Benue Trough of Nigeria Using High**  
2                                    **Resolution Aeromagnetic Data**

3                                    Ogunmola J.K, Ayolabi E.A and Olobaniyi S.B

4  
5                                    Department of Geosciences, University of Lagos

6                                    **ABSTRACT**

7 The Yola Arm is the east-west trending part of the Upper Benue Trough made up of Cretaceous  
8 sediments that are Albian to Maastrichtian in age. This work involves interpreting satellite  
9 imagery and aeromagnetic data to map out structures within the basin and estimate the depth  
10 to the magnetic basement which could be an aid to further exploratory work in the basin. The  
11 SPOT 5 imagery covering the basin was processed and interpreted and lineaments extracted  
12 from it. The digital elevation model (DEM) of the area was also used to extract the drainage  
13 pattern of the area and as an aid in mapping the lineaments that are visible on the surface. The  
14 geomagnetic field of the earth was removed from the aeromagnetic data using the IGRF-12  
15 model. The vertical derivative (VDR) enhanced the high frequency and short wavelength  
16 components of the data which could be volcanics. The source parameter imaging (SPI)  
17 technique which works well at all magnetic latitudes and the spectral analysis were applied to  
18 the data to estimate the sediment thickness within the basin. A low pass filter with a cut-off  
19 wavelength of 1000 meters was applied to the data to remove the high frequency short  
20 wavelength component of the data after which the tilt derivative (TDR) was computed to  
21 enhance anomalies that may be faults on the underlying basement. The lineaments from the  
22 SPOT 5 data show a predominant NNE-SSW, NE-SW followed by the NNW-SSE with a few N-S  
23 and E-W trends and the TDR of the aeromagnetic data show a predominantly NE-SW trend  
24 which is the predominant trend in the Benue Trough while a few strike in the N-S,NW-SE, and  
25 WNW-ESE direction. This suggests that the basin was subjected to several stress regimes.  
26 Differential uplift of the basement fault blocks may have given rise to drape folds observed in  
27 the overlying sediments. The depths to the magnetic basement range from about 1 km to about  
28 4.3 km with the deepest part in the eastern part of the Basin. The depth analysis indicates that  
29 the Cretaceous sediments are thick enough to generate hydrocarbons.

30     **Keywords:- SPOT 5, GIS, Aeromagnetic data, Faults/Lineaments, Geology**

## 31 **1.0 Introduction**

32 The Upper Benue Trough (Fig 1) of Nigeria is comprised of three basins: the east–west trending  
33 Yola Basin (Yola Arm), the north-south trending Gongola Basin (Gongola Arm) and the  
34 northeast-southwest trending Lau Basin (Main Arm). The Benue Trough is itself a product of the  
35 West and Central African Rift System in which it opened as a broad strike-slip fault system. The  
36 continents (South America, Africa, Arabia, Madagascar, India, Australia and Antarctica) are  
37 thought to have been one super continent called Gondwanaland and the relative movement of  
38 the continental plates resulted in the formation of a triple junction where only two arms of the  
39 junction opened into the ocean and the third arm did not. The Benue trough is thought to be  
40 the failed arm of the triple junction which also led to the separation of the African and the  
41 South American plates (Burke et al 1970). This present work is an attempt to understand the  
42 structural framework and the geometry of the basin which can be an aid to further exploratory  
43 efforts in the basin. It involves processing and interpreting high resolution magnetic data  
44 collected at 400 meters flight line spacing by Fugro Airborne surveys which is an improvement  
45 on past interpretations that were done with the old data that was collected in 1972 at 2 km  
46 flight line spacing. This improvement in data quality will give a better understanding of the  
47 basin and also give more accurate depth to basement values. This study is aimed at showing the  
48 effectiveness of integrating remote sensing, magnetic and other ancillary data within a GIS for  
49 geological/structural studies. When interpreting aeromagnetic data, it is necessary to compare  
50 structures or magnetic anomalies delineated from the derivatives with the surface features as  
51 can be seen from aerial photographs or satellite images. Remote sensing has become a widely  
52 accepted research tool by geologists the world over. It gives the overview required to construct  
53 regional unit maps, useful for small scale analyses, and planning field traverses to sample and  
54 verify various units for detailed mapping. It is also used to understand the spatial distribution  
55 and surface relationships between rock units. For this study SPOT 5 image with a spatial  
56 resolution of 5 meters was used. Satellite imagery can give us a picture of the surface where  
57 outcrops and features such as dykes can be observed. Also rock units and geological structures  
58 often show a strong correlation with relief and can be mapped with a detailed topographic

59 analysis. Digital Elevation Models (DEM) are used for such analysis to derive topographic  
60 attributes such as elevation, slope, aspect, shaded relief, drainage network, etc with the aid of a  
61 Geographic Information System (GIS).

62 Magnetic data interpretation can be used to establish the relationship between basement  
63 tectonics and the overlying structures within the sediments. The 1<sup>st</sup> vertical derivative is a  
64 vertical gradient method that uses a Fast Fourier Transform (FFT) to enhance the high  
65 frequency component of a magnetic field made up of intrusives and volcanics while suppressing  
66 the low frequency content which is due to the regional field. The tilt-derivative (TDR) is a  
67 powerful method because of its peculiar characteristics and it was used to enhance the  
68 basement faults. It attempts to equalize the amplitude output of TM anomalies across a grid. All  
69 other derivatives have an amplitude response that is closely linked to the amplitude of the TMI  
70 anomaly but the TDR is independent of amplitude of the anomaly and are instead controlled by  
71 the reciprocal of the depths of the magnetic sources. It is also a good signal discriminator in the  
72 presence of noise. The Source Parameter Imaging (SPI) technique so called because all the  
73 parameters that make up the source which include depth, dip and susceptibility contrast are  
74 computed from the complex analytical signal was used for this study because the technique  
75 assumes only induced magnetization and works well at all magnetic latitudes which makes it a  
76 good choice for the Yola basin that is at low magnetic latitude. The spectral analysis method  
77 was also used for this study in order to compare with the estimates from the SPI because it has  
78 the advantage of being able to filter out noise from data without losing information during the  
79 process.

80 In the Northern Gulf of Mexico, Alexander (1999) integrated magnetic, gravity, seismic and  
81 refraction data to map out the geometry of the basement and was able to map out grabens and  
82 the horst structures within the basin and also identified the primary faults within the basement  
83 and the secondary faults in the overlying sediments. In the past, interpretations of magnetic  
84 data was done using data with a 2 km flight line spacing that can only resolve structures of > 4  
85 km resolution but recent data acquired can resolve structures as low as 400 meters which will  
86 give a better interpretation of the basin. Understanding the deformation that occurred within

87 the basement can help understand the resultant deformation and stratigraphy of the basin.  
 88 This present work attempts to interpret aeromagnetic data with the aid of ancillary data such as  
 89 satellite imagery and digital elevation model (DEM) to map out the basement geometry and  
 90 structures within the basin which can be an aid for further detailed exploratory work.

91

## 92 2.0 Geological setting

93 The area of study forms part of the Upper Benue Trough of Nigeria (fig 1) which is a product of  
 94 the West and Central African Rift System where it opened as a broad strike-slip fault system  
 95 (Binks and Fairhead 1992).

96

97

98

99

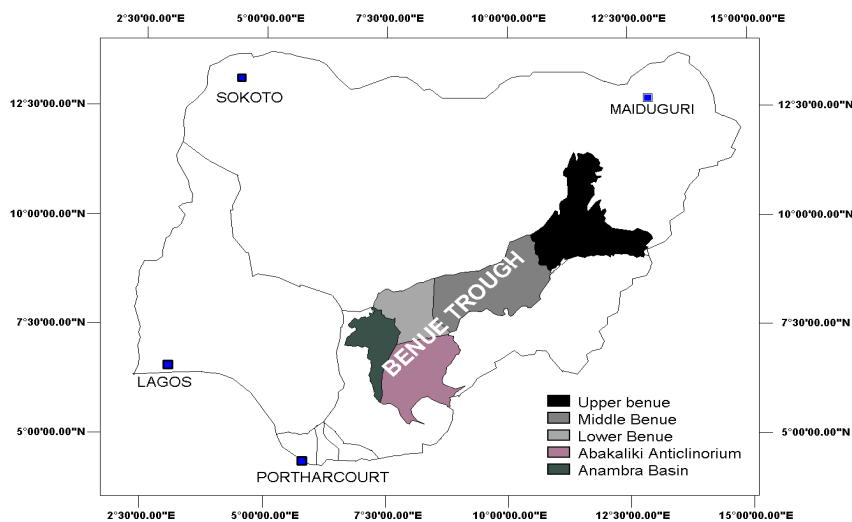
100

101

102

103

104

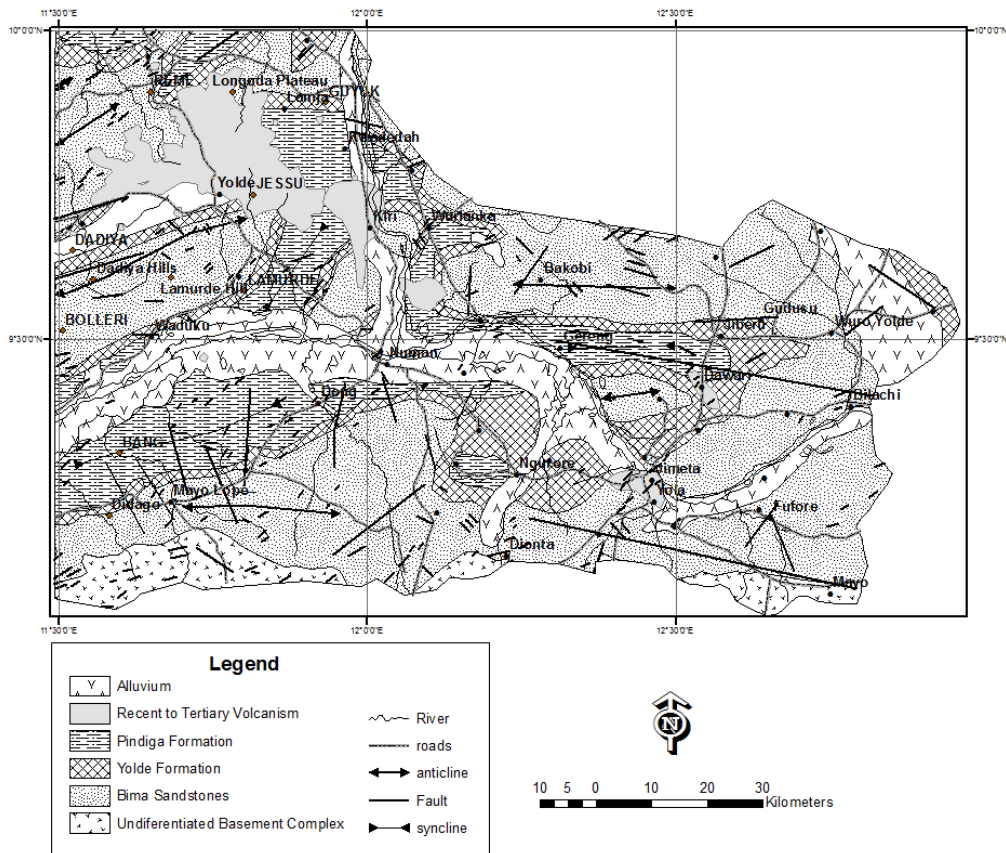


105 Figure 1. Map of Nigeria showing the major subdivisions of the Benue Trough (after Ologun et al,2008)

106

107 The area falls within latitude  $9^{\circ} 03' N$  to  $10^{\circ} 00' N$  and longitude  $11^{\circ} 30' E$  to  $13^{\circ} 00' E$ . It covers  
 108 an area of about  $12000 \text{ km}^2$ . The geology consists of crystalline basement, Cretaceous  
 109 sediments and volcanics (fig2).





110 Figure 2. Geological Map of the Yola Basin (modified from Benkheilil, 1989, NGSA map,2004)

111

112 A horst and graben structure which resulted in variation in sedimentary thickness of between 2-  
 113 3 km was deduced from interpretation of aeromagnetic data of the lower Benue (2 km flight  
 114 line spacing). It also revealed a major lineament trend of NE-SW (Obi et al, 2008). Okereke et al,  
 115 (2012) observed a major NE-SW lineament trend from Landsat data which is similar to the NE-  
 116 SW trend of linear structures interpreted from magnetic data. A sedimentary thickness of about  
 117 4 km was also deduced for the sub-basin. The depth to basement in the Garoua basin (also  
 118 known as the Yola rift) which is an eastward extension of the Benue trough in North Cameroon  
 119 was found to vary from 4.4 km to 8.9 km (Mouzong et al, 2014) from spectral analysis of  
 120 residual gravity data. Horizontal gradient method also revealed deep faults that trend in a  
 121 major NW-SE direction within the basin. The spectral analysis and horizontal gradient method  
 122 of aeromagnetic data of the Upper Benue Trough revealed a maximum sedimentary thickness

123 of 3.45 km, a depth to shallow sources of about 1.5 km and a major structural trend of NE- SE,  
124 ENE- WSW and WNW- ESE in order of abundance (Alagbe and Sunmonu, 2014). Results from  
125 spectral analysis of the aeromagnetic data of the area around the Longuda Plateau (Upper  
126 Benue Trough) indicate a maximum sedimentary thickness of about 2620m and shallow  
127 magnetic sources of about 670 m (Kasidi and Ndatuwong, 2008). Fairhead and Okereke (1987)  
128 determined the crustal thickness of the Benue Trough and the Yola basin as about 24 km and 19  
129 km respectively from gravity profiles while Stuart et al (1985) determined a crustal thickness of  
130 23 km for the Cameroon extension of the Yola basin. Salako and Udensi (2013) determined  
131 sedimentary thickness to vary between 0.268 km and 3.35 km for parts of the Upper Benue  
132 Trough from spectral analysis of magnetic data. Ogunmola et al (2015) observed from high  
133 resolution magnetic data that the dominant structural trend in the underlying basement of the  
134 Middle Benue Trough is NE-SW.

135

## 136 **2.1 Crystalline Basement**

137 The crystalline basement is made up of scattered remains of well metamorphosed sedimentary  
138 rocks and diverse, mostly granitic, plutonic masses that are collectively called older Granites  
139 (Carter et al, 1963). They are seen to occur extensively south of the Benue where they emerge  
140 from beneath the Bima sandstone. Three phases of the Older granites have been distinguished;  
141 basic and intermediate plutonic rocks, fine grained granites and syntectonic granites. The  
142 earlier rocks have also gone through granitization that emplaced tracts of granitic migmatites  
143 and hybrid rocks.

144

## 145 **2.2 Cretaceous Sediments**

146 The Cretaceous sediments in the Upper Benue Trough are sandwiched between the  
147 Precambrian-Late Paleozoic basement gneisses and granites that occur as inliers in some places  
148 such as the Kaltungo Inlier. Overlying the Precambrian basement rocks is the Albian Bima



149 sandstone which is the oldest Cretaceous sediment in the Upper Benue. It is overlain by the  
 150 transitional Cenomanian-Turonian Yolde Formation which is succeeded by the Pindiga  
 151 Formation (Turonian-Coniacian) with the Gongila Formation in the Gongola Basin and the  
 152 Dukul, Jessu, Sekuleye and Numaha Formations as its lateral equivalents in the Yola Basin (Table  
 153 1). These successions are succeeded by the Gombe sandstone (Campanian-Maastrichtian) in the  
 154 Gongola Basin and the Lamja sandstone as its lateral equivalent in the Yola Basin. The  
 155 succession is capped by the Tertiary Kerri-Kerri Formation west of Gombe in the Gongola Basin.

156

### 157 2.2.1 Lithostratigraphic units of the Yola basin

158 A generalized stratigraphic chart of the Cretaceous Formation of the Yola basin is shown in  
 159 table 1.

160 Table 1. Generalized Stratigraphic Chart of the Cretaceous Formation of the Yola basin (modified from Zaborski et  
 161 al., 1997; Obaje et al., 2004).

162

163

AGE	YOLA BASIN
MAASTRICHTIAN	LAMJA SANDSTONE
CAMPANIAN	
SANTONIAN	
CONIACIAN	NUMANHA FORMATION
TURONIAN	SEKULEYE FORMATION
CENOMANIAN	JESU FORMATION
	DUKUL FORMATION
	YOLDE FORMATION
ALBIAN	BIMA SANDSTONE
PRE-CAMBRIAN	BASEMENT COMPLEX

170

171

172

### 173 **2.3 Cretaceous Volcanics**

174 Most of the minor volcanic activity that occurred during the Upper Cretaceous is within the  
175 Benue Trough (Carter et al, 1963). In the Yola arm, they can be seen in a stream 5.5 km NW of  
176 Chikala within the Lamja sandstone. They are also present at about 2 km west of Lamja and in  
177 the Numanha river within the Numanha shales. In the Jessu Formation, they are seen in a  
178 stream near Chikila and in the southern part of Dukul and Kunini. Within the Dukul Formation,  
179 they occur about 1.6 km North of Dadiya and at about 5 km east of Reme on the Talasse road.  
180 Within the Bima, they are seen at the Lamurde anticline where the basalts have been  
181 weathered to greyish green clays. Most of the volcanics consist of thin lavas and tuffs.

182

### 183 **2.4 Tertiary to Recent Volcanics**

184 The Late Tertiary and Quaternary witnessed a major epoch of volcanic activity during which  
185 numerous volcanic plugs were emplaced and also saw the building of the great lava Plateau of  
186 Biu and Longuda. Majority of the plugs consist of fine-grained olivine basalts with a few being  
187 trachytic and phonolitic in composition. They are found within all the Cretaceous Formation.  
188 The Longuda lavas are mostly fine grained olivine basalts and reach their maximum thickness of  
189 240, 275 and 305 meters at Dukul, Jou and Kola respectively.

190

## 191 **3.0 Materials and Methods**

### 192 **3.1 Data Available**

193 **Magnetic data-** The data set used for this study is an aeromagnetic survey that was acquired at  
194 a flight line spacing of 400 meters and a terrain clearance of 80 meters surveyed by Fugro  
195 Airborne surveys for the Federal Government of Nigeria. The data study is in grid format only.  
196 The earth's geomagnetic field was removed from the data using the IGRF 12 Model.

197 **SPOT 5 Data-** For this study, SPOT 5 data with a ground resolution of 5 meters was used. This  
198 coverage offered by SPOT-5 is a key asset for applications such as medium-scale mapping (at  
199 1:25 000 and 1:10 000).

200

201 **Digital Elevation Model (DEM)-** The DEM data set for this study is from the SRTM (shuttle  
202 Radar Topography mission) flown by NASA that obtained digital elevation models of the earth's  
203 surface. The SRTM data of the Yola basin was downloaded from the Global Land Cover Facility  
204 (GLCF).

205

### 206 **3.2 Reduction to the Pole (RTP) or Reduction to the Equator (RTE)**

207 The RTP method of reducing maps made anywhere, with exception of those at low latitudes,  
208 into what they would appear like if the inclination of the magnetic field were 90 degrees  
209 described by Baranov (1957) is a standard method used when interpreting magnetic data  
210 because at the poles, magnetic anomalies are true reflections of the geologic bodies causing  
211 them. It has however been observed that amplitude correction at very low latitudes ( $\pm 10^\circ$ ) for  
212 north-south trending features distorts magnetic anomalies and unreasonable amplifies  
213 noise/artefacts (McLeod et al, 1993). The magnetic data can also be reduced to the equator  
214 (RTE) such that the magnetic bodies will appear horizontal at the equator (Leu ,1982) . The  
215 structure will show the same anomaly shape as those at the poles. His approach recalculates  
216 the total magnetic intensity assuming the magnetic body is lying in a horizontal position and  
217 anomaly lows are converted to magnetic highs by reversing the phase by 180 at the same  
218 location over the middle of the bodies. At very low latitudes, it is also unlikely for a RTE to make  
219 any significant change in the data as was observed in the Yola basin with a declination of -2.011,  
220 and inclination of -3.413 (from the IGRF 12 Model) which showed a resultant grid that is similar  
221 to the TMI grid. In the light of all the above, the original TMI grid of the Yola basin was used for  
222 data enhancement and interpretation.

### 223 3.3 1<sup>st</sup> Vertical Derivative

224 The 1<sup>st</sup> vertical derivative,  $dT/dz$  is a vertical gradient method that uses a Fast Fourier Transform  
225 (FFT) to enhance the high frequency component of a magnetic field made up of intrusives and  
226 volcanics while suppressing the low frequency content which is due to the regional field (Paine,  
227 1986). The transformation takes place in the spectral phase therefore the accuracy cannot be  
228 determined but the frequency domain can show the level of accuracy of the method. The first  
229 vertical derivative (VDR) can be viewed as taking measurements of the total magnetic intensity  
230 (TMI) at two locations that are a small distance above each other at the same time and dividing  
231 the difference in the TMI values with the vertical distance between them (Milligan and Gunn  
232 1997). A first vertical derivative transform was applied to the TMI grid of the study area.

233

### 234 3.4 Tilt derivative

235 The TDR was used in this study to enhance anomalies that could be basement faults. The tilt-  
236 derivative (TDR) is useful because of some of its peculiar characteristics. It tends to equalize the  
237 amplitude output of TMI anomalies across a grid. While other conventional derivatives show  
238 amplitude response that is closely linked to the amplitude of the TMI anomaly, the TDR is  
239 independent of amplitude of the TMI anomaly but controlled by the reciprocal of the depths of  
240 the sources (Verduzco et al., 2004). The TDR also shows a maximum that peaks over the  
241 anomaly. Because the  $\tan^{-1}$  component of the TDR is restricted to + 1.57 and – 1.57, it acts like  
242 an automatic gain control (AGC) filter that amplifies the amplitude of signals that are low which  
243 makes the Tilt derivative a powerful method. Since an average depth of 1 km depth to shallow  
244 magnetic sources for the Upper Benue has been estimated by several authors (Alagbe and  
245 Sunmonu 2014, Okereke et al, 2012, Kasidi and Ndatuwong 2008), a low pass filter with a cut-  
246 off wavelength of 1000 meters was applied to the data to reduce the high frequency short  
247 wavelength component of the data after which this transform was applied to the TMI data of  
248 the study area.

249 **3.5 Topographic Analysis-** Using the spatial analyst in ArcMap, several topographic attributes  
250 such as shaded relief, curvature, slope, flow direction and stream network were derived from  
251 the digital elevation model (DEM).

252

### 253 **3.6 Structural Mapping**

254 The first stage of the structural mapping was to distinguish which of the high frequency  
255 components of the data derived from the first vertical derivative are due to surface/subsurface  
256 geology or due to cultural noise from the environment. This was carried out with the aid of  
257 SPOT 5 image and the SRTM data of the study area. The SPOT 5 data was passed through edge  
258 enhancement image processing method using the ERDAS Imagine software so as to sharpen the  
259 surface geological features and give a good contrast between the settlements which appear as  
260 cyan colour and the surrounding pixels due to vegetation or water. The next stage of structural  
261 mapping involved mapping out on-screen lineaments observed from the SPOT 5 image. It also  
262 involved mapping out magnetic lineaments that could be due to the contacts between two rock  
263 types of contrasting magnetic susceptibility or edges of structures that could be faults or  
264 intrusives within the sediments. To achieve this, all the various data sets were displayed in  
265 ArcMap and by studying one layer at a time and comparing with other layers in the GIS  
266 environment. The geological map was useful because it showed the location where the  
267 basement occurs as surface exposure. The SRTM data was able to show the outline of surface  
268 geological features such as dikes which was also evident on the SPOT 5 image. One of the  
269 advantages of working in a GIS environment using several data sets is the opportunity to  
270 examine features that are spatially referenced. A feature that is less pronounced in one data set  
271 can be more pronounced in another data. A shapefile was created in ArcCatalog after which the  
272 magnetic lineaments were digitized on-screen.

273

274

### 275 **3.7 Depth to Basement Inversion from Magnetic data**

276 One of the objectives of this research is to derive estimates of depth to causative bodies in  
277 parts of the Yola Basin which will also give us the thickness of the overlying sediments. The  
278 methods used include the Local wavenumber/source parameter imaging (SPI) and spectral  
279 analysis.

### 280 **3.8 Local wavenumber**

281 This method developed by Thurston and Smith (1997) also known as the Source Parameter  
282 Imaging (SPI) technique is so called because all the parameters that make up the source which  
283 include depth, dip and susceptibility contrast are computed from the complex analytical signal.  
284 Fairhead et al (2004) related the source depth to the local wavenumber ( $k$ ) of the magnetic field  
285 which can be derived from the calculated total horizontal and vertical gradients of the RTP grid.  
286 The technique works well at all magnetic latitudes which makes it a good choice for the Yola  
287 Basin that is at low magnetic latitude. One other advantage of this method is that the depth  
288 estimates can be gridded and exported from geosoft to ArcGIS where it can be overlain on the  
289 geological and structural maps derived from the magnetic derivatives. Using the SPI method in  
290 geosoft, the depth estimates were derived from the TMI data of the Yola basin that was upward  
291 continued a distance of 1km to minimize signals from the high frequency and short wavelength  
292 component of the data. The number of peaks to be detected was set at 3 or 4 directions and  
293 the maximum depth of solutions was set at 6000m meters based on well data and earlier depth  
294 estimates derived from the basin by other authors. The depth solutions were saved in a  
295 database and the terrain clearance of 80 meters and 1 km upward continued distance was  
296 deducted after which it was gridded using the minimum curvature method.

297

### 298 **3.9 Spectral Analysis**

299 When gravity or magnetic sources occur in cluster at a certain depth, the sources will be shown  
300 as a straight line that has a gradient of  $-4\pi$  in a power spectrum which is the plot of the

301 logarithm of the amplitude of the source against the wavenumber (Spector and Grant, 1970).  
302 Therefore different straight-line branches in a power spectrum show the existence of clusters  
303 of gravity or magnetic sources at the different depths. This process of identifying signals from  
304 different sources known as Spectral Analysis was carried out in geosofts magmap by first  
305 carrying out a Fast Fourier Transform on the data before computing the radially averaged  
306 power spectrum. The area was divided into 19 spectral blocks. Block 1-15 about 27.5km by  
307 27.5km while block 16-19 are about 35km by 27.5 km each and block 19 is 20km by 27.5km.  
308 From the SPOT 5 data folds such as the Lamurde Anticline are seen to be more than 10 km wide  
309 and about 20 km in length. The anomalies in the magnetic data also range from a few  
310 kilometers wide to about 24 km wide in the south-eastern part of the basin. It is in the light of  
311 the aforementioned that a size of 27.5 km x 27.5 km was deemed suitable for most of the  
312 spectral blocks. The \*.SPC energy files were imported into Microsoft excel. A matlab code was  
313 compiled which plots the power spectrum after which the linear segments were then drawn.  
314 The program determines the slope of the linear segments and hence depth for the two sources.

315

### 316 **3.10 Depth to Basement Map**

317 A depth to basement map of the Yola basin was produced from the depth estimates that were  
318 derived from the Local wavenumber and spectral analysis and the structures extracted from the  
319 structural mapping using the Tilt derivative. The basement faults were displayed in ArcMap and  
320 the following data sets were overlain on them-

321 - depth solutions from the SPI method

322 - depths from the spectral analysis

323 A shapefile was created and using the editor tool, polylines were drawn beside and within the  
324 structures without any overlaps and were given depth values based on geologically reasonable  
325 depths from the various depth estimate methods.



326 The polylines were then converted to points using the ET Geowizard in ArcGIS and stored as a  
327 point data set which contains all the attributes of the polyline. The points were then  
328 interpolated using the Spatial Analyst extension that performed a spline with barriers on the  
329 point data using a minimum curvature spline method. The barriers in this case are the  
330 basement faults represented as polyline features. The interpolated output was exported to  
331 Geosoft Oasis Montaj where it was displayed as database table and gridded using the minimum  
332 curvature method to produce the depth to basement map of the study area. The depth to  
333 basement map was displayed in ArcMap and the faults overlaid on it. Contours of the depth to  
334 basement map were also extracted and overlain on the depth to basement structure map for  
335 better visualization of the basement configuration.

336

#### 337 **4.0 Results and Discussion**

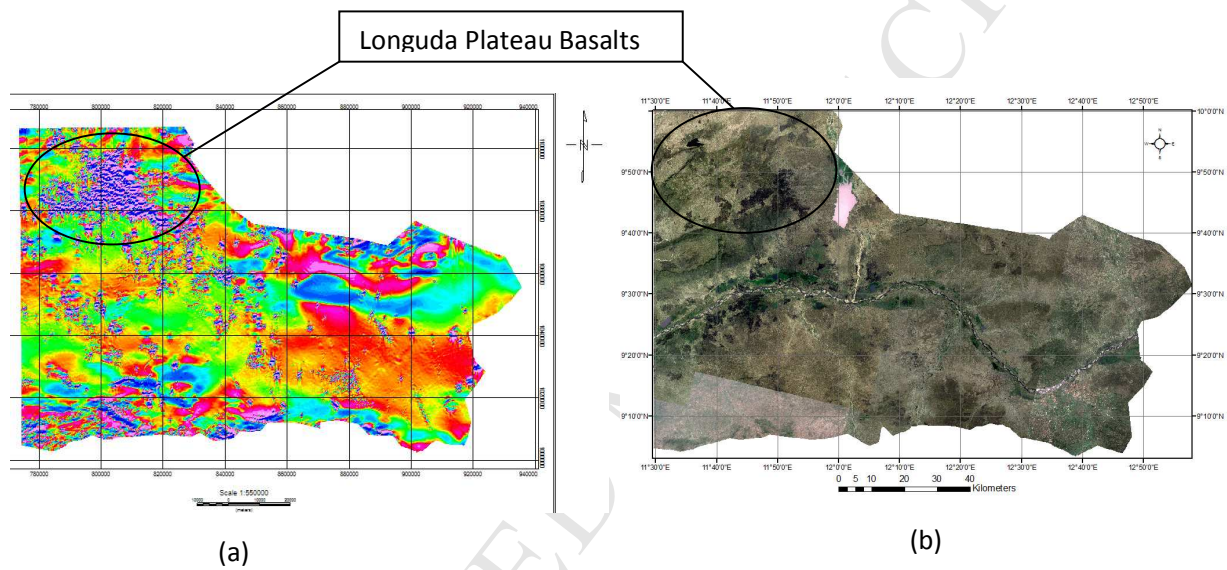
338 The integration of the tilt derivative and vertical derivative was very useful in understanding the  
339 geology of the basin. The VDR showed that some of the high frequency and low wavelength  
340 components are due to surface/subsurface geology most likely volcanics. A good example can  
341 be seen in the north-eastern part of the basin (fig 3) where the VDR clearly defined the outline  
342 of the Longuda Plateau which is basaltic. There was a strong correlation between the south-  
343 western edges of the Longuda Plateau (olivine basalts) observed from the SPOT 5 image and  
344 the outline of the high frequency and short wavelength components observed from the VDR  
345 grid. There was also a strong correlation with some of the surface exposures of tertiary basalts  
346 observed during field work. These include those on the western part of Waduku and the  
347 southern part of Kwadedah. It was therefore possible properly map out the outline of the  
348 Plateau and other volcanics within the basin as shown in the geological map (fig 2). The root of  
349 the Longuda basalts may also extend farther southwards below the sandstones of the Lamurde  
350 hill.

351 The drainage network derived from the topographic analysis using the digital elevation model  
352 (DEM) from the SRTM is dendritic which is indicative of alluvial rocks.

353 The major structural trend observed from SPOT 5 imagery is also NNE-SSW, NE-SW followed by  
 354 the NNW-SSE with a few N-S and E-W trends (fig 5) and they range in length from 200 m to  
 355 about 16 km. These trends have also been observed from Landsat study (Ananaba and  
 356 Ajakaiye, 1987) and interpretation of SPOT 5 imagery (Ogunmola et al, 2014). The straight limbs  
 357 of the folds in the basin such as the Lamurde anticline as seen from the SPOT 5 image trend in a  
 358 NE-SW direction.

359

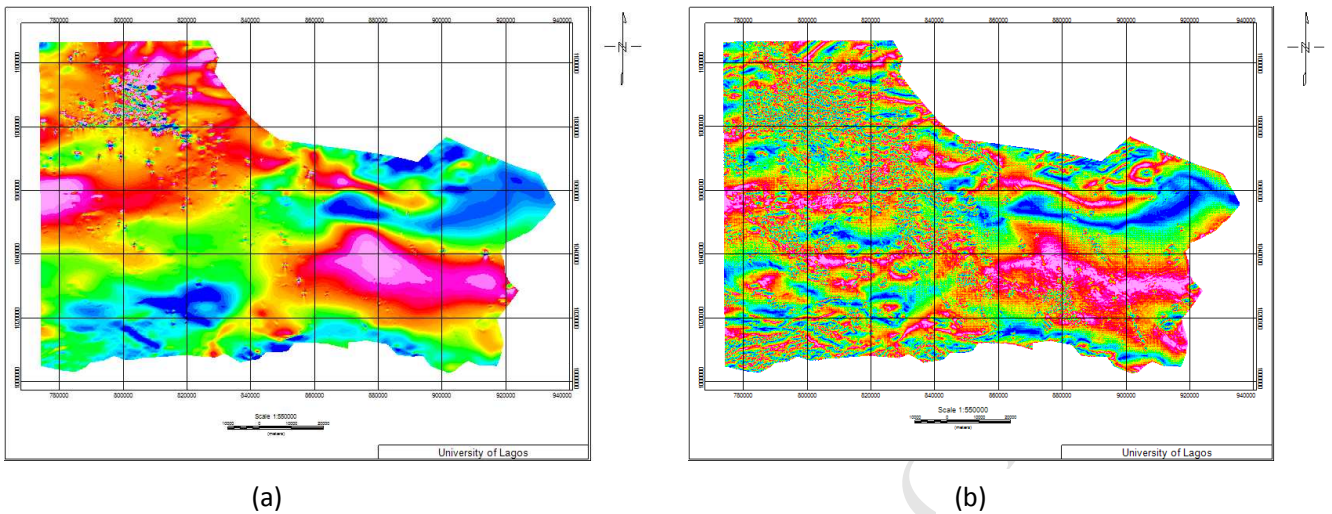
360



361

362 Figure 3. 1<sup>st</sup> Vertical Derivative of the magnetic data (a) and Satellite imagery of the study area (b)

363



365 Figure 4. The TMI of the magnetic data (a) and the Tilt derivative (b)

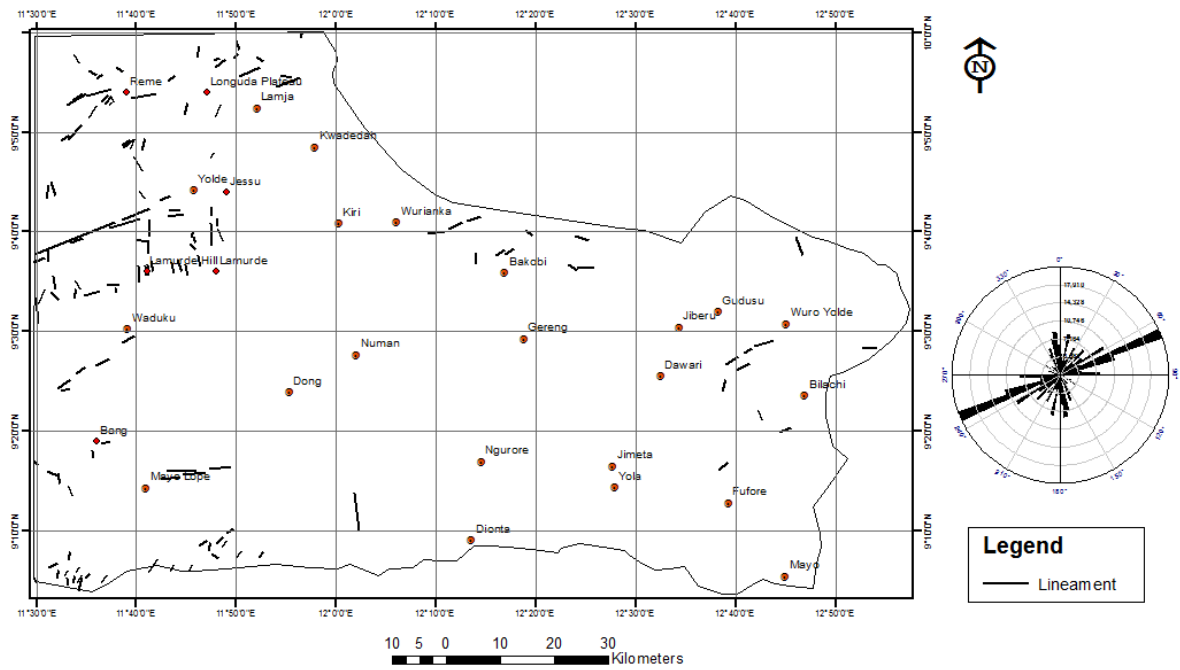
366 The Tilt derivative shown in fig 4 (b) clearly shows that this method is obviously very good at  
 367 enhancing the basement faults because the zero crossing of the Tilt derivative closely delineate  
 368 the edges of structures. It was able to enhance structures that were not observed from earlier  
 369 studies. These structures were also observed not to cut across the tertiary basalts such as on  
 370 the Longuda Plateau which suggests that the movements within the underlying basement  
 371 ceased before the Tertiary. The dominant trend of these faults was found to be in the NE-SW  
 372 with a few N-S, NW-SE, and WNW-ESE direction (fig 6) and range in length from 0.8 km to more  
 373 than 58 km. These trends have also been observed from surface outcrops (Guiraud, 1990) and  
 374 from geophysical and remote sensing data (Benkhelil, 1987,1989, Ogunmola et al,2015). These  
 375 basement faults may be related to fracture zones such as the Romanche fracture zones and the  
 376 Chain and Charcot fracture zones which are thought to have continental extensions and are  
 377 likely to control the major NE-SW fracture system along the Benue Trough as suggested by  
 378 earlier authors (Wright, 1976). A remarkable feature in the western part of the Yola basin are  
 379 two faults that are about 32 km apart and are parallel to each other. These faults trend WNW-  
 380 ESE for more than 58km and may well extend into the Garoua Basin in Cameroon and is  
 381 overlain by the Cretaceous sediments. Sandwiched between these faults is a zone of positive  
 382 anomaly and corresponds to areas delineated as the deepest part of the study area from the  
 383 source parameter imaging (SPI) and the spectral analysis (~3.7 km). The rock types on the

384 surface are the limestones, shales and clay of the Yolde Formation, hence this zone can be said  
385 to be the area with the thickest Cretaceous deposits. This zone stretches for about 60 km and is  
386 about 30 km wide. Gravity surveys by Osazuwa et al (1981) also delineated this zone along a N-  
387 S profile. The positive anomaly observed in this zone may be due to basic intrusives with high  
388 magnetite content at the surface of the magnetic basement or contributions from high  
389 frequency-low wavelength intrusives as amplified around Jimeta and south of Fufore and  
390 Dawari. The structures within the sediments may have originated from crustal stresses that  
391 were transmitted through incompetent sediments in directions different from the major  
392 tectonic trend of the underlying basement. Compressional events such as the one in the  
393 Santonian (80ma) that reactivated pre-existing shear zones in the Benue Trough (Benkhelil et  
394 al,1989) can lead to the formation of the NNW-SSE, N-S and E-W trends observed within the  
395 sediments. These faults are later than the folding that produced the great folds of the Benue  
396 Trough such as the Dadiya syncline and the Lamurde anticline which may be related to deep  
397 seated movements in the underlying basement. Some of these structures observed from the  
398 SPOT 5 image include the straight limbs of the folds around Dadiya that stretch for about 16 km  
399 and those around the southern part of Reme but most of the lineaments within the sediments  
400 are less than 1.5km in length. The difference in stress directions observed on the overlying  
401 sediments and those observed on the underlying basement suggests that they passed through  
402 different stress regimes.

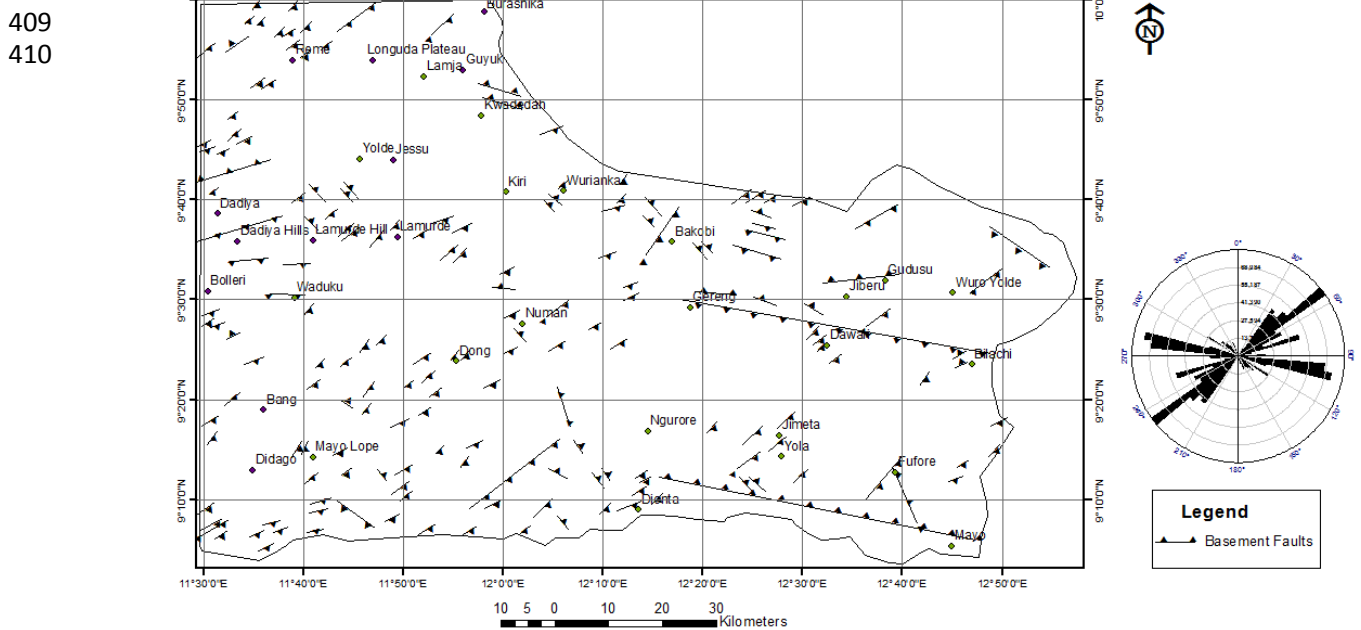
403

404

405



406 Figure 5. Lineaments extracted from SPOT 5 image of study area and a Rose diagram showing the distribution of  
 407 lineaments by direction and weighted by length  
 408



409  
 410  
 411 Figure 6. Faults derived from Tilt derivative (TDR) of study area and Rose diagram showing the distribution of faults  
 412 by direction and weighted by length  
 413

414  
415

416

417

418

419

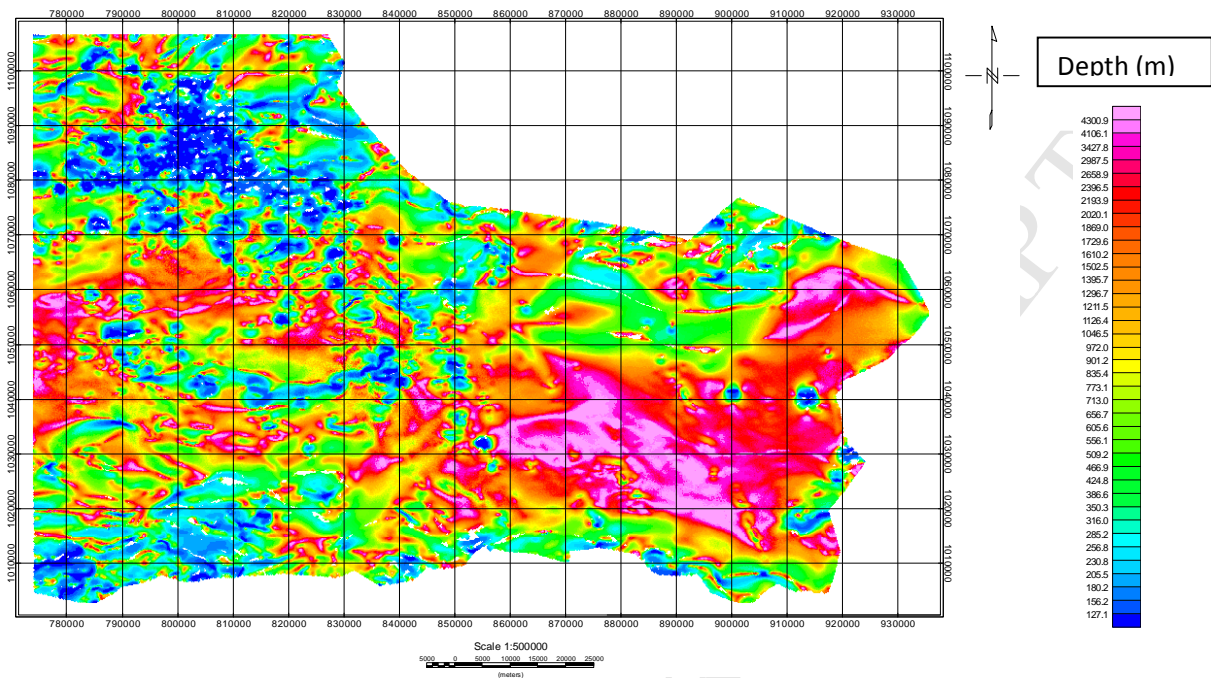
420

421

422

423

424



425

Figure 7. A grid of depth estimates from magnetic sources derived from the SPI method

426

427

428

429

430

431

432

433

434

435

436

437

438

The grid of the depth solutions derived from the Source Parameter Imaging is shown in fig 7. The depths range from about a 0.127 km to about 4.3 km with the deepest part being in the eastern part of the basin. These depths are from all magnetic sources that include shallow volcanics/intrusives mainly in the northern part of the basin and shallow basement rocks on the southern part. The 19 plots of the log of spectral energy versus the wave number are shown in fig 8 and fig 9 and the depths derived from the spectral analysis are shown in table 2. The shallow depths which could be due to intrusives and volcanics range from about 0.343 km around Bang and Didago to 0.70 km around Yola but are mainly confined to the western part of the basin. The second depths which are most likely mainly from the magnetic basement range from about 1 km southwest of Yola to about 3.66 km around Yolde and Bilachi.



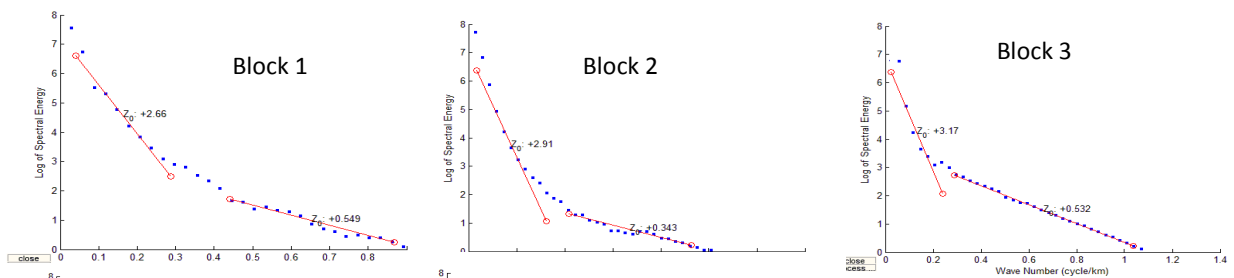
439

440

441

442

443

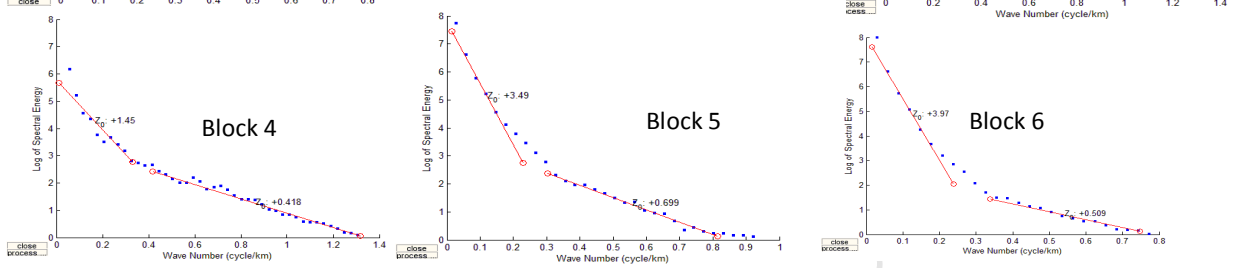


444

445

446

447



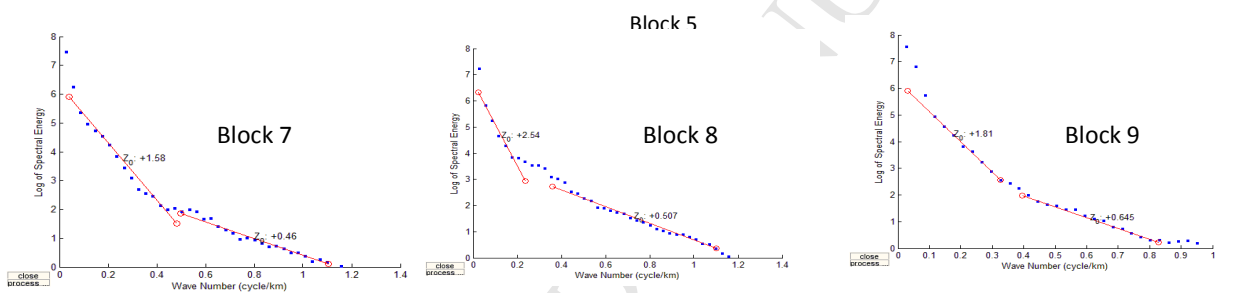
448

449

450

451

452



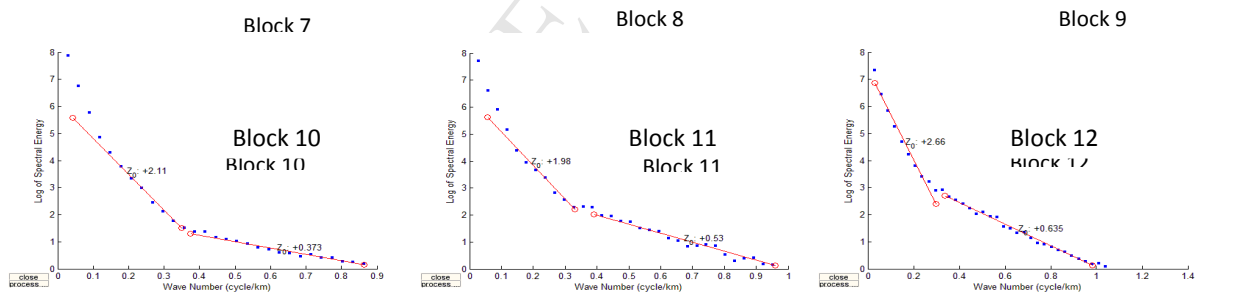
453

454

455

456

457



458

459

460

461

462

Figure 8. Spectral plots of energy against frequency for spectral blocks 1-12



463

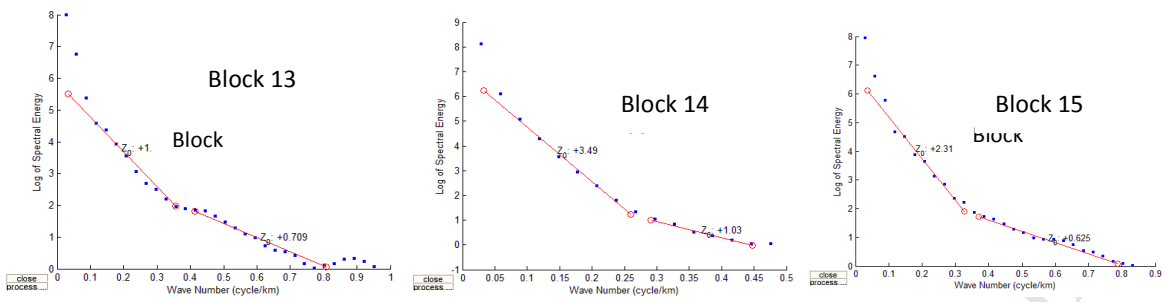
464

465

466

467

468



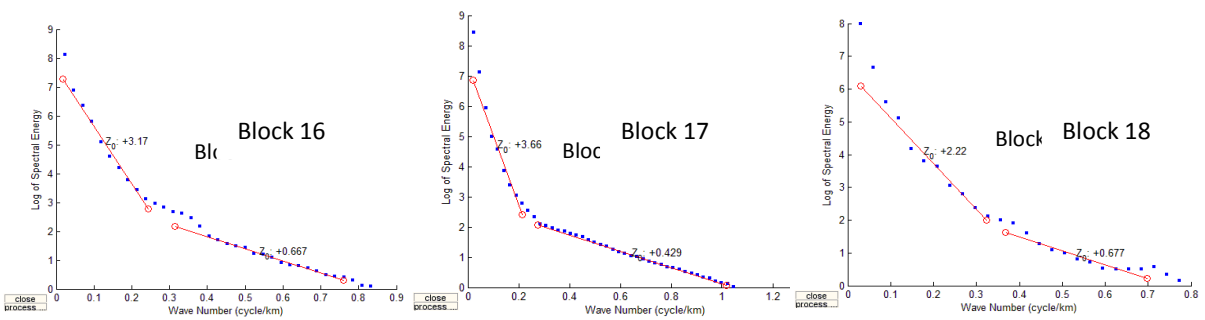
469

470

471

472

473



474

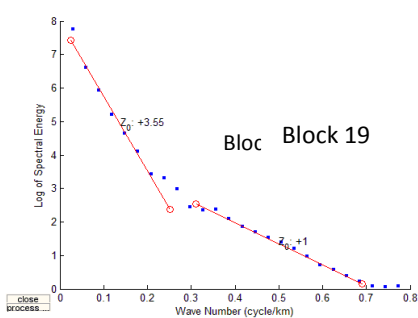
475

476

477

478

479



480

481

482

483

484

485

486

Figure 9. Spectral plots of energy against frequency for spectral blocks 13-19

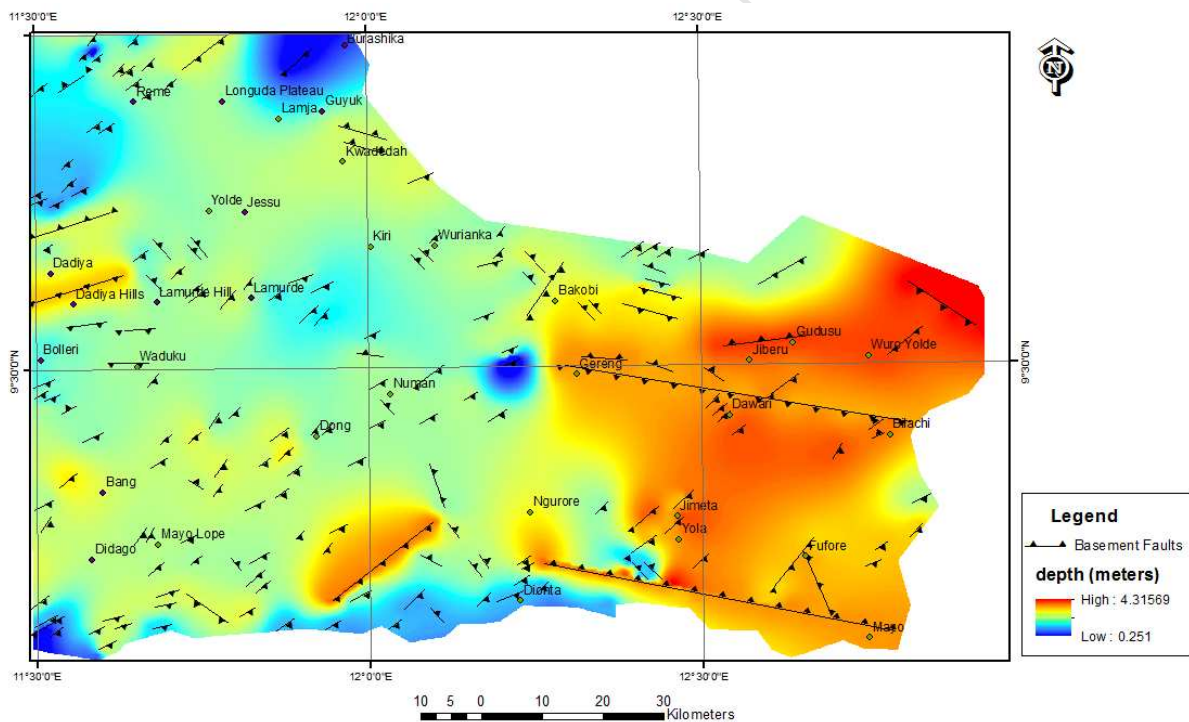
487 **Table2:** Estimated depth to the shallow magnetic sources (depth1) and deep magnetic sources (depth2) in km

Spectral Block	Longitude	Latitude	Depth 1 (km)	Depth 2 (km)
Block 1	11.5-11.75	9.0-9.25	0.549	2.66
Block 2	11.5-11.75	9.25-9.5	0.343	2.91
Block 3	11.25-11.75	9.5-9.75	0.532	3.17
Block 4	11.25-11.75	9.75-10	0.418	1.45
Block 5	11.75-12	9.0-9.25	0.699	2.49
Block 6	11.75-12	9.25-9.5	0.509	2.97
Block 7	11.75-12	9.5-9.75	0.460	1.58
Block 8	11.75-12	9.75-10	0.507	2.54
Block 9	12-12.25	9.0-9.25	0.645	1.81
Block 10	12-12.25	9.25-9.5	0.373	2.11
Block 11	12-12.25	9.5-9.75	0.530	1.98
Block 12	12-12.25	9.75-10	0.635	2.66
Block 13	12.25-12.30	9.0-9.25	0.709	1.00
Block 14	12.25-12.30	9.25-9.5	1.03	2.49
Block 15	12.25-12.30	9.5-9.75	0.625	2.31
Block 16	12.5-12.825	9.0-9.25	0.667	3.17
Block 17	12.5-12.825	9.25-9.5	0.429	3.66
Block 18	12.5-12.825	9.5-9.75	0.667	2.22
Block 19	12.825-13.0	9.5-9.75	1.00	3.55

488

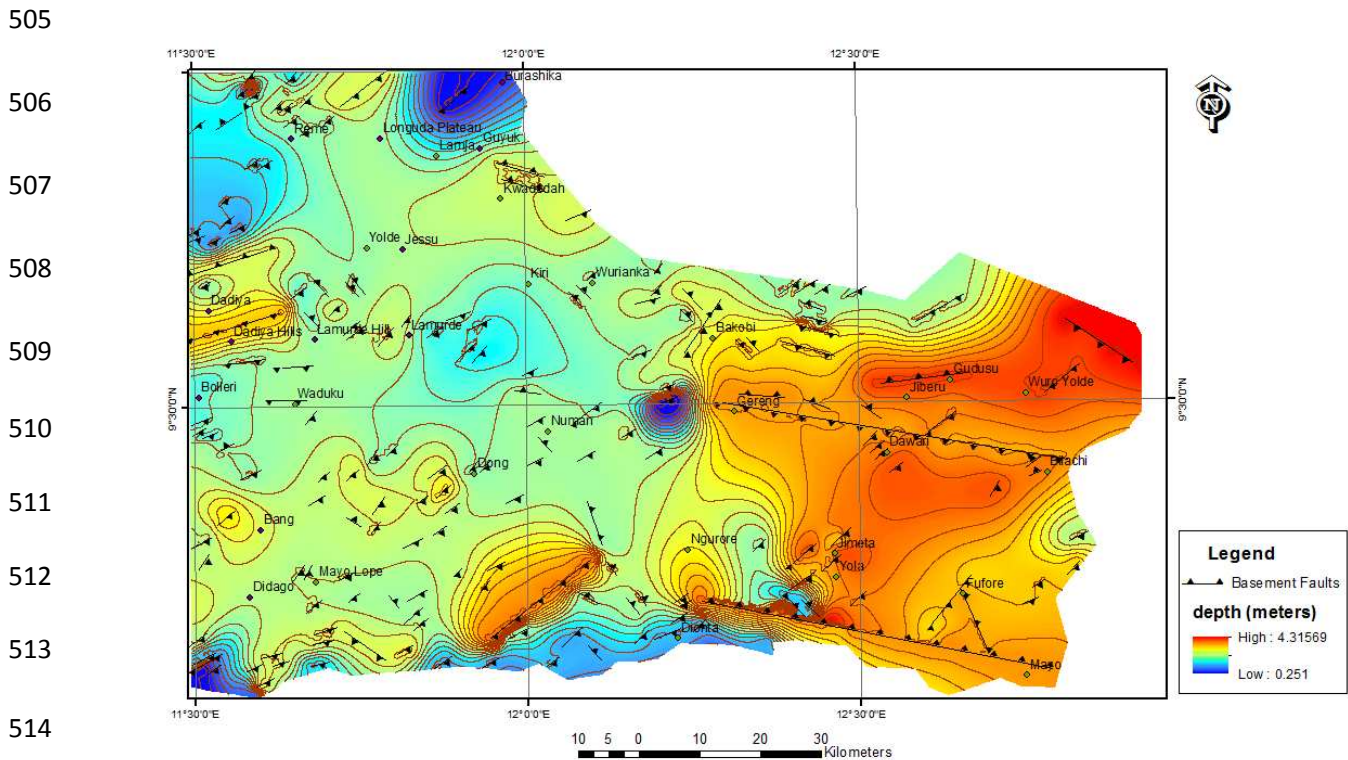
489 Generally, the depth estimates from the local wavenumber (LWV) or source parameter imaging  
490 (SPI) method and those from the spectral analysis show some correlation. Depths are taken as  
491 depth to the magnetic sources.

492 Both estimates show that the eastern half of the Yola basin is the deepest starting from Bakobi  
 493 to Yolde in the northern part and from Ngurone through Jimeta to Fufore in the south as shown  
 494 by the depth to basement maps (fig 10 & 11). However the SPI gave the deepest average  
 495 estimate of about 4.3 km while the spectral analysis gave about 3.66 km. These depths are  
 496 similar to those derived from recent study of the Yola basin such as about 3.4 km from spectral  
 497 analysis of aeromagnetic data (Salako and Udensi, 2013), sedimentary thickness of about 4 km  
 498 (Okereke et al, 2012) and a depth of about 4.4 km in the Garoua basin which is the eastern  
 499 extension of the Yola basin in Cameroon (Mouzung et al, 2014). The depth to basement  
 500 structure maps (fig 10 & 11) gives a better visualization of configuration of the basement. Most  
 501 of the faults are deep seated within the underlying basement while the shallow ones occur  
 502 where there are surface exposures of the basement.



503 Figure 10. Depth to Basement structure map of the Yola Basin

504



515 Figure 11. Depth to Basement structure Map of the Yola Basin with an overlay of the depth contours

516

## 517 5.0 Conclusions

518 This interpretation has shown that the underlying basement in the Yola basin is faulted in a  
 519 major NE-SW direction and these basement faults may have controlled the fracture system with  
 520 the Cretaceous sediments that may have been generated in the Precambrian. Wright (1981)  
 521 suggested that it was differential uplift of the basement fault blocks that gave rise to drape  
 522 folds in the overlying sediments. He based his conclusion on the evidence from the straight  
 523 limbs of the Lamurde anticline that trend in a NE-SW direction as observed from ERTS imagery  
 524 which could be surface expressions of large basement faults. Evidence is now at hand from this  
 525 study to support his theory because the Tilt derivative was able to show a major basement fault  
 526 that runs parallel to the straight limbs of the Lamurde anticline. Other conclusions drawn from  
 527 this interpretation are-

- 528 1. The dominant trend of the basement faults was found to be in the NE-SW with a few N-  
529 S, NW-SE, and WNW-ESE directions that may have been generated in the Precambrian.
- 530 2. These basement faults may be related to fracture zones such as the Romanche fracture  
531 zones and the Chain and Charcot fracture zones which are thought to have continental  
532 extensions and are likely to control the major NE-SW fracture system along the Benue  
533 Trough.
- 534 3. The major structural trends within the sediments as observed from SPOT 5 imagery and  
535 geological mapping are also NNE-SSW, NE-SW followed by the NNW-SSE with a few N-S  
536 and E-W trends.
- 537 4. The major direction of the great Lamurde fold in the basin are in the NE direction which  
538 suggests that some of the folding may be related to the deep seated earth movements  
539 of the underlying basement.
- 540 5. The presence of some NNE-SSW, NE-SW followed by the NNW-SSE with a few N-S and E-  
541 W structures in the sediments suggests that they were as a result of stresses that were  
542 post Cretaceous.
- 543 6. The area may have undergone several stress regimes.
- 544 7. The absence of faults that are abundant in the underlying basement in the great Tertiary  
545 basalts of the Longuda Plateau suggests that the tectonic regimes ceased before the  
546 Tertiary.
- 547 8. Apart from the Tertiary basalts of the Longuda Plateau, localised volcanics are present in  
548 parts of the study area especially to the west.
- 549 9. The deepest part of the basin is found in the south-eastern part of the area where the  
550 Cretaceous sediments are about 4 km thick and are flanked by two prominent faults.
- 551 10. The Cretaceous Sediments in the eastern part of the basin are thick enough for  
552 hydrocarbon generation.

### 553 **Acknowledgements**

554 This study has benefited from the facilities provided by the National Centre for Remote Sensing,  
555 Jos, Nigeria.

556 **References**

557 Alagbe, O.A. and Sunmonu, L.A., 2014, Interpretation of Aeromagnetic Data from Upper Benue  
558 Basin, Nigeria Using Automated Techniques. *IOSR Journal of Applied Geology and Geophysics*  
559 *(IOSR-JAGG). Volume 2, Issue 5 , PP 22-40*

560

561 Alexander, M., 1999, "Northern Gulf of Mexico basement architecture: Crustal study to  
562 prospect leads". Paper presented at the 1999 Society of Exploration Geophysics sixty-Ninth  
563 Annual meeting workshop: The seismic link: Reducing Risk, Houston, TX.

564

565 Ananaba S.E and Ajakaiye D.E., 1987, Evidence of tectonic control of mineralization in Nigeria  
566 from Lineament density analysis. A landsat study. *Journal of Remote Sensing*, vol 8 No 10,p  
567 1445.

568

569 Baranov, V., 1957, A new method for interpretation of aeromagnetic maps: Pseudo-gravimetric  
570 anomalies: *Geophysics*, 22, 359-383.

571

572 Barber, W., Tait, E.A. and Thomson, J.H., 1954, The geology of the lower Gongola. *Ann Rept.*  
573 *Geol. Surv. Nigeria*, 1952-53, 18-20.

574

575 Benkheilil, J., 1987, Cretaceous deformation, magmatism and metamorphism in the Lower  
576 Benue Trough, Nigeria, *Geological Journal* 22 (Thematic issue) 467-493.

577

578 Benkheilil, J., 1989, The origin and evolution of the Cretaceous Benue Trough (Nigeria). *Journal*  
579 *of African Earth Sciences*. Vol. 8, Nos, 2/3/4. pp. 251-282.

580 Binks, R.M, and Fairhead, J.D., 1992, A plate tectonic setting for Mesozoic rifts of West and  
581 Central Africa . *Tectonophysics*, 213 (1992) 141-151.

582

583 Burke, K.C., Dessauvage, T.F.J. and Whiteman, A.J., 1970, Geological history of the Benue valley  
584 and adjacent areas. In: T.F.J. Dessauvage (Editor), *African Geology*, University of Ibadan Press,  
585 Ibadan.

586

587 Carter, J.D., Barber, W., Tait, E.A., Jones, G.P., 1963, The Geology of Parts of the Adamawa,  
588 Bauchi and Borno provinces in Northwestern Nigeria, *Geol Surv. Nigeria Bull.* 30: 53 – 61.

589

590 Fairhead J.D and Okereke C.S., 1987, A regional gravity study of the West African rift system in  
591 Nigeria and Cameroon and its tectonic interpretation. *Tectonophysics*, 143. 141-159.

592

593 Fairhead, J. D., Williams S. E. and Flanagan, G., 2004, Testing magnetic local wavenumber  
594 depth estimation methods using a complex 3D test model: 74th Annual International Meeting,  
595 SEG, Expanded Abstracts, 742–745.

596

597 Gunn, P.J, 1975, Linear Transformations of Gravity and Magnetic Fields, *Geophysical*  
598 *Prospecting* 23, 300-312.

599

600 Guiraud, M., 1990, Tectono-sedimentary framework of the early Cretaceous Continental Bima  
601 Formation (Upper Benue Trough, NE Nigeria), *Journal of African Earth Sciences*, 10 (1/2), 341-  
602 353.

603



- 604 Kasidi, S. and Ndatuwong, L.G., 2008, Spectral Analysis of Aeromagnetic Data Over Longuda  
605 Plateau and Environs, North-Eastern Nigeria. *Continental J. Earth Sciences* 3:28 – 32.
- 606
- 607 Leu, L., 1982, Use of reduction-to-the-equator process for magnetic data interpretation:  
608 *Geophysics*, 47, 445.
- 609
- 610 Macleod, I.N., Veira, S., Chaves, A.C., 1993, Analytical signal and reduction-to-the-pole in the  
611 interpretation of total magnetic field data at low magnetic latitudes, *Proceedings of the third*  
612 *international congress of the Brazilian society of geophysicists*.
- 613
- 614 Milligan P.R and Gunn P.J 1997, Enhancement and presentation of airborne geophysical data.  
615 *AGSO Journal of Australian Geology & Geophysics*, 17(2), 63-75.
- 616
- 617 Mouzong, M.P , Kamguia, J., Nguiya, S., Shandini, Y. and Manguelle-Dicoum, E., 2014,  
618 Geometrical and structural characterization of Garoua sedimentary basin, Benue Trough, North  
619 Cameroon, using gravity data. *Journal of Biology and Earth Sciences*. ISSN: 2084-3577
- 620
- 621 Nwajide C.S, 2013, *Geology of Nigeria's Sedimentary Basins*. CSS Bookshops Ltd, Lagos, P. 565.
- 622
- 623 Obaje, N.G., Wehner, H., Scheeder, G., Abubakar, M.B., Jauro, A., 2004, Hydrocarbon  
624 prospectivity of Nigeria's Inland Basins: From the view point of organic geochemistry and  
625 organic petrology. *American Association of Petroleum Geologists Bulletin* 88, 325–353.
- 626

627 Obi, D. A., Okereke, C. S., Obi, E. O. and George, A. M., 2008, "Mapping depth to the crystalline  
628 basement in the lower Benue Trough (Nigeria) using Power Spectrum and horizontal gradient  
629 magnitude techniques on aeromagnetic data". International journal of Natural and Applied  
630 Sciences (IJNAS), vol. 3, Nos. 102 P. 69 – 74.

631

632 Ojo J.O. and Akande O.S., 2000, Depositional Environments and Diagnosis of the Carbonate  
633 Facies of Dukul and Jessu Formations in the Yola Basin N.E. Nigeria: Implications for Reservoir  
634 Potential. NAPE Bulletin V. 15. No. 1. P. 47 – 59.

635

636 Ogunmola J.K , Ayolabi E.A, and Olobaniyi S.B., 2014, Lineament Extraction From Spot 5 And  
637 Nigeriasat-X Imagery Of The Upper Benue Trough, Nigeria. The International Archives of the  
638 Photogrammetry, Remote Sensing and Spatial InFormation Sciences, Volume XL-1,ISPRS  
639 Technical Commission I Symposium, 17 – 20 November 2014, Denver, Colorado, USA.

640

641 Ogunmola, J.K. , Gajere, E.N., Ayolabi, E.A., Olobaniyi, S.B., Jeb, D.N. and Agene, I.J., 2015,  
642 Structural study of Wamba and Environs, north-central Nigeria using aeromagnetic data and  
643 NigeriaSat-X image. Journal of African Earth Sciences 111 307-321.

644

645 Okereke, C. N., Onu, N.N., Ibe, K.K., Selemo, A.O.I., Opara, A.I., Ikoro, D.O., Ibeneme, S.I. & Oha,  
646 I.A., 2012, Analysis of Landsat and Aeromagnetic Data For Mapping of Linear Structures: A Case  
647 Study of Yola Area, Upper Benue Trough, Nigeria. International Journal of Engineering Research  
648 and Applications (IJERA) ISSN: 2248-9622 Vol. 2, Issue 3, pp.1968-1977.

649

- 650 Ologun J.A.A, Ogezi A.E.O, Ogunmola J.K, and Alaga A.T, 2008, The Application of Remote  
651 Sensing and GIS Techniques in Evaluating Airborne Radiometric Anomaly around Wamba  
652 Nassarawa Egon Area, North Central Nigeria. Nigerian Jour. of Space Research 5: 95 – 114.  
653
- 654 Osazuwa, I.B., Ajakaiye, D.E. and Verheijen, P.J.T., 1981, Analysis of the structure of Part of the  
655 Upper Benue Rift Valley on the Basis of New Geophysical Data. Earth Evolution Sciences 2: 126-  
656 135.  
657
- 658 Paine, J.W., 1986, A comparison of methods for approximating the vertical gradient of one-  
659 dimensional magnetic field data, Geophysics, 51 (9), 1725-1735.  
660
- 661 Salako, K. A., Udensi, E. E., 2013, Spectral Depth Analysis of Parts of Upper Benue Trough and  
662 Borno Basin, North-East Nigeria, Using Aeromagnetic Data. International Journal of Science and  
663 Research (IJSR), India Online ISSN: 2319-7064  
664
- 665 Spector, A., and Grant, F.S., 1970, Statistical models for interpreting aeromagnetic data.  
666 Geophysics, vol 35 pp 293-302.  
667
- 668 Stuart, G.W., Fairhead, J.D., Dorbath, L. and Dorbath, C.,1985, A seismic refraction study of the  
669 crustal structure associated with the Adamawa Plateau and Garoua Rift, Cameroon, West  
670 Africa. Geophys. J.R. Astron. Sot., 81: 1-12.  
671
- 672

- 673 Thurston, J. B., and Smith R. S., 1997, Automatic conversion of magnetic data to depth, dip,  
674 susceptibility contrast using the SPI™ method: *Geophysics*, 62, 807–813.  
675
- 676 Verduzco, B., Fairhead, J. D., Green, C. M. and MacKenzie, C. 2004, New insights into magnetic  
677 derivatives for structural mapping: *The Leading Edge*, 23, 116–119.  
678
- 679 Wright, J.B., 1976. Fracture systems in Nigeria and initiation of fracture zones in the south  
680 Atlantic. *Tectonophysics* 34, T43-T47.  
681
- 682 Zaborski, P., Ugoduluwa, F., Idornigie, A., Nnabo, P., and Ibe, K., 1997, Stratigraphy and  
683 structure of the Cretaceous Gongola basin, northwest Nigeria. *Bull. de Centre des Recherches*  
684 *Exploration Production Elf– Aquitaine*. 21, 153–186.

### Highlights

1. The dominant trend of the basement faults was found to be in the NE-SW with a few N-S, NW-SE, and WNW-ESE directions that may have been generated in the Precambrian.
2. The major structural trends within the sediments as observed from SPOT 5 imagery and geological mapping are also NNE-SSW, NE-SW followed by the NNW-SSE with a few N-S and E-W trends.
3. Differential uplift of the basement fault blocks may have given rise to drape folds observed in the overlying sediments.
4. The area may have undergone several major stress regimes that ceased before the Tertiary.
5. Apart from the Tertiary basalts of the Longuda Plateau, localised volcanics are present in parts of the study area especially to the west.
6. The deepest part of the basin is found in the south-eastern part of the area where the Cretaceous sediments are about 4 km thick and are flanked by two prominent faults.